




**Ionization and recombination times of the long trajectory in high-order harmonic generation**Shengjun Yue <sup>1,2,3</sup>, Yangyang Li,<sup>1,2</sup> Shan Xue,<sup>1,2,\*</sup> Hongchuan Du <sup>1,2,†</sup> and Manfred Lein <sup>3</sup><sup>1</sup>*Frontiers Science Center for Rare Isotopes, Lanzhou University, Lanzhou 730000, China*<sup>2</sup>*School of Nuclear Science and Technology, Lanzhou University, Lanzhou 730000, China*<sup>3</sup>*Leibniz University Hannover, Institute of Theoretical Physics, Appelstraße 2, 30167 Hannover, Germany*

(Received 12 May 2022; accepted 29 July 2022; published 26 August 2022)

Measuring the ionization and recombination times in high-order harmonic generation driven by strong laser fields is of fundamental importance in attosecond science and vital for assessing the temporal accuracy of trajectory-resolved high-harmonic spectroscopy. We investigate the effect of the electron-core interaction on the ionization and recombination times of the long trajectory in high-order harmonic generation. Using a classical model and the analytical  $R$ -matrix theory for helium, it is found that the attractive interaction leads to a 30-as shift of the ionization times for the long trajectory. By numerically solving the time-dependent Schrödinger equation for a helium atom model, we demonstrate that this small time shift can be probed by using orthogonally polarized two-color fields with high probe frequencies.

DOI: [10.1103/PhysRevA.106.023117](https://doi.org/10.1103/PhysRevA.106.023117)**I. INTRODUCTION**

The interaction between strong laser pulses and matter offers a unique combination of semiclassical physics and quantum mechanics in a nonstationary setting. After an electron tunnels out of the potential barrier induced by a strong field acting on an atom or molecule, the electron motion is nearly classical and therefore it can be described in terms of trajectories [1,2]. For a linearly polarized field, the released electron oscillates due to the alternating force, and it may return to the parent ion. This recollision may cause recombination leading back into the ground state, accompanied by emission of high-frequency radiation. This process is known as high-order harmonic generation (HHG). The above-described mechanism is reflected in the classical three-step model [1,3] and in the quantum-mechanical strong-field approximation (SFA) [4]. Every HHG trajectory is associated with certain values of the ionization time, the recombination time, and the return energy of the electron, which determines also the radiated photon energy. In each optical cycle of the driving femtosecond laser pulse, the ionization and recombination times vary over only a fraction of the cycle. Therefore, the photon energy can be mapped to the ionization and recombination times on an attosecond timescale and HHG offers possibilities to study physical phenomena with attosecond temporal resolution [5–10]. Importantly, several distinct trajectories may give rise to the same photon energy. For a given photon energy, there are two relevant trajectories per optical half cycle, known as the short and the long trajectory. Roughly, long trajectories start just after a peak of the electric field and the excursion time is between three-quarters of a cycle and a full period. Short trajectories start later than the

long trajectories and return earlier. In experiments, it is common that the long trajectory is suppressed by the macroscopic phase mismatching conditions [11]. In this case, a one-to-one map between photon energy and time (up to multiples of a half cycle) is realized.

High-harmonic spectroscopy (HHS) is the field of research that aims at studying properties of matter by observing the high-harmonic radiation. For example, HHS has been used to study molecular structure [12–14], vibrational dynamics of molecules [15–18], and multielectron dynamics [19–21]. For applications of time-resolved HHS, it is essential to know the ionization and recombination times accurately. One way of measuring these times is based on orthogonally polarized two-color (OTC) fields. Such tailored fields have been widely used to control and monitor electron wave packets [22–29]. Time measurements with OTC fields are applicable to both HHG [30,31] and photoelectron emission [32–35]. In the OTC scheme for HHG, a weak cross-polarized probe field (or streaking field) with higher frequency is added to the strong fundamental field to perturb the electron trajectory in the lateral direction. The intensities of the high-order harmonics and the recombination angles of the trajectories change with the relative phase of the two fields, i.e., the two-color delay. The variations of these two observables have been termed displacement gate and velocity gate, respectively [30]. For each harmonic order, i.e., for each given frequency of the emitted radiation, measuring these two independent observables enables us to extract both ionization and recombination times. The time-retrieval method was generalized from real-time to complex-time trajectories in Ref. [31]. Using  $\omega$ - $2\omega$  two-color fields together with the complex-time method, the retrieved ionization and return times match well with the quantum-orbit (QO) model [2], which neglects the Coulomb interaction between the electron and the parent ion. This might create the impression that these times are unaffected by the Coulomb interaction. However, the analytical  $R$ -matrix (ARM) theory

\*xuesh@lzu.edu.cn

†duhch@lzu.edu.cn

predicts that the ionization time exhibits a significant time shift of dozens of attoseconds caused by the electron-ion interaction [36]. This shows that the previous  $\omega$ - $2\omega$  approach is not reliable for retrieving the ionization time with few-attosecond precision. Recently, it was shown that using a high-frequency (e.g.,  $4\omega$ ) probe field instead of the  $2\omega$  probe field solves this problem [37]. These calculations were carried out for the short HHG trajectory and they revealed a Coulomb-induced 35-as shift towards earlier times [37]. The retrieved times matched well with the ARM prediction and also with results from a classical model including the Coulomb interaction.

Although research on the long trajectory is not as common, we note that the short and long trajectories have been successfully separated in a number of experiments [6,18,38,39]. The long trajectory provides a different time-detection window for trajectory-resolved HHS. This makes the long trajectory attractive for attosecond-scale time-resolved studies. The effects of the Coulomb interaction on the ionization time of the long trajectory have only been investigated within classical trajectory models so far [40,41]. The classical trajectory Monte Carlo simulations of [40] did not find any Coulomb time shifts, possibly due to the specific initial conditions and recombination conditions, in particular the choice of zero longitudinal initial velocity. With initial conditions taken from the SFA, including the nonzero velocity at the tunnel exit, ionization was found to take place earlier than in the QO model [41].

In this article, we use solutions of the time-dependent Schrödinger equation (TDSE) for a helium atom model to demonstrate the OTC-based reconstruction of ionization and emission times for the long trajectory in HHG. Similar to the case of the short trajectory [37], we find that the Coulomb potential causes an ionization-time shift towards earlier times. For the long trajectory, this shift is accurately measurable when employing probe frequencies of five times the fundamental frequency or more. In contrast, when using low probe frequencies, the retrieved ionization time is in good agreement with the Coulomb-free QO model, because low-frequency streaking fields, together with the established retrieval equations, are blind to the effects of Coulomb interaction on the ionization times [35,37].

The article is organized as follows. Section II outlines the details of the TDSE, the Gabor time-frequency analysis, and the OTC-based time-retrieval method. Section III applies the retrieval method to the long trajectory and analyzes the effect of the Coulomb potential on the ionization times. Section IV summarizes our work.

## II. THEORETICAL MODEL

### A. Time-dependent Schrödinger equation

We use a single-active-electron model to describe the interaction of strong fields and a helium atom. In this model, the motion of the electron with coordinate  $\mathbf{r}$  is limited to two-dimensional space. The TDSE for the electron wave function  $\psi(\mathbf{r}, t)$  in the length gauge reads (Hartree atomic units are used unless otherwise stated)

$$i\frac{\partial}{\partial t}\psi(\mathbf{r}, t) = \left(-\frac{\nabla_{\mathbf{r}}^2}{2} + V(\mathbf{r}) + \mathbf{r} \cdot \mathbf{E}(t)\right)\psi(\mathbf{r}, t). \quad (1)$$

Here  $V(\mathbf{r}) = -1/\sqrt{\mathbf{r}^2 + a}$  is a soft-core potential with  $a = 0.0684$  a.u., which reproduces the ionization potential  $I_p = 24.6$  eV of helium. The OTC field  $\mathbf{E}(t) = -\dot{\mathbf{A}}(t)$  is described by the vector potential

$$\mathbf{A}(t) = -\frac{E_0}{\omega}f(t)\left(\sin(\omega t)\hat{\mathbf{e}}_x + \frac{\epsilon}{n}\sin(n\omega t + \phi)\hat{\mathbf{e}}_y\right), \quad (2)$$

where  $\hat{\mathbf{e}}_x$  and  $\hat{\mathbf{e}}_y$  are unit vectors,  $E_0$  and  $\omega$  are the peak field amplitude and frequency of an 800-nm fundamental laser field with intensity  $4.0 \times 10^{14}$  W/cm<sup>2</sup>, respectively, and  $\phi$  is the relative phase between the fundamental field and the streaking field, also termed two-color delay. The real positive number  $n$  determines the streaking frequency  $n\omega$ . In the TDSE simulations, the OTC field has a trapezoidal envelope  $f(t)$  that ranges from  $-T$  to  $2T$  ( $T = 2\pi/\omega$ ) with one-cycle ramps. To suppress contributions to HHG from the edges of the laser pulse, a steep function  $\cos^6(\omega t/4)$  is taken as the leading edge of  $f(t)$  in the interval  $-T \leq t \leq 0$  and the falling edge in the interval  $T \leq t \leq 2T$  has the form  $\cos^6[\omega(t - T)/4]$ . For the probe field, we choose the relative amplitude  $\epsilon = 0.02$ .

Because the calculation allows us to select the HHG from one half cycle (discussed below), we can easily use noninteger values of  $n$  as well as integer values. In the case of an experiment with commonly used multicycle pulses, one would use integer  $n$  to ensure that the timing of the probe field relative to the fundamental field is the same in every optical cycle.

The two-dimensional TDSE is numerically solved using the Crank-Nicolson method [42,43] with the time step  $\Delta t = 0.05$  a.u. The box size is  $L_x \times L_y = 280 \times 100$  a.u. with  $2800 \times 1000$  grid points. At each time step, the wave function is multiplied with mask functions to avoid reflections from the boundary. The mask function along the  $x$  axis is  $F(x) = \cos^{1/8}[\pi(|x| - x_0)/(L_x - 2x_0)]$  for  $|x| \geq x_0$  and  $F(x) = 1$  for  $|x| \leq x_0$  with  $x_0 = 7L_x/18$ . In the  $y$  direction, a similar treatment is applied, where  $y_0$  is set to  $7L_y/18$ . Once the wave function has been obtained, the dipole acceleration  $\mathbf{a}(t)$  with components  $a_x(t)$  and  $a_y(t)$  is calculated via the Ehrenfest theorem [44],

$$\mathbf{a}(t) = \langle \psi(\mathbf{r}, t) | \partial_{\mathbf{r}} [V(\mathbf{r}) + \mathbf{r} \cdot \mathbf{E}(t)] | \psi(\mathbf{r}, t) \rangle. \quad (3)$$

### B. Gabor transform

One challenge in the numerical simulations is that the harmonic spectrum cannot be used to determine the ionization and recombination times directly, since one harmonic order has contributions from several trajectories. In other words, the harmonic order does not correspond to a unique pair of ionization time and return time. In experiments, short or long trajectories can be selected by appropriate choice of the phase-matching conditions in the laser-gas interaction zone. To separate the trajectories in the calculated single-atom response, we consider the time-frequency profile of the harmonic emission. In the previous calculations for short trajectories [37], this method was used in combination with a suitably chosen absorber that suppresses the long trajectories due to their large spatial extent. In the present work, our aim is to keep the information on the long trajectory. Therefore, the absorbing mask starts further away from the center and we rely completely on the time-frequency analysis to separate the trajectories. To this end, we use the Gabor transform [8,10,31].

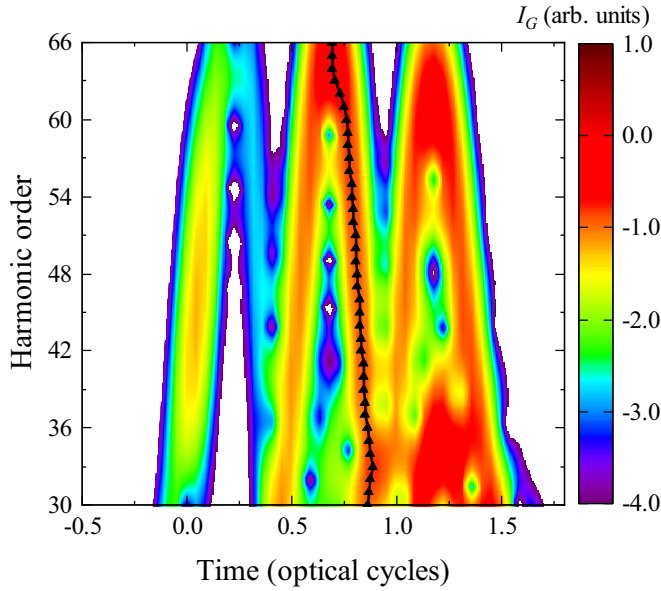


FIG. 1. Gabor time-frequency profile of the harmonic emission, calculated according to Eq. (4), resulting from the  $\omega$ - $2\omega$  laser pulse with an intensity of  $4.0 \times 10^{14}$  W/cm<sup>2</sup> and fundamental wavelength 800 nm. The two-color delay is zero. The triangles connected by the black line show the local maxima of the Gabor distribution for the long trajectory.

The total harmonic signal for both possible polarization directions ( $x$  and  $y$ ), resolved in time and frequency, reads

$$I_G(\Omega, t) = I_{Gx}(\Omega, t) + I_{Gy}(\Omega, t) = \sum_{j=x,y} \left| \int dt' a_j(t') e^{-\frac{(t'-t)^2}{2\sigma^2} + i\Omega t'} \right|^2, \quad (4)$$

where we use  $\sigma = 1/(3\omega)$ . The indices  $x$  and  $y$  denote the  $x$  and  $y$  components. For a given harmonic frequency  $\Omega$ , we find the local maximum of the time-dependent function  $I_G(\Omega, t)$  in the range  $t \in [0.7T, 1.0T]$ , where the long-trajectory signal is located. To illustrate the procedure, Fig. 1 shows an example of a Gabor time-frequency distribution with black triangles indicating the positions of the local maxima at integer harmonic orders. The temporal positions  $t_e$  of these maxima are used to obtain the long-trajectory harmonic intensity as  $I_G(\Omega, t_e)$  and the amplitude ratio between the  $y$  and  $x$  components as  $R = \sqrt{I_{Gy}(\Omega, t_e)/I_{Gx}(\Omega, t_e)}$ . These two observables depend on the two-color delay  $\phi$ , which is the basis for the time-retrieval method. Note that the times  $t_e$  are only used to obtain from the TDSE solutions the two described observables, which are analogous to what is measured in the experimental implementation [30]. The times  $t_e$  are not used as a “measured” return time. In the following, we focus on harmonic orders from 47 to 60 due to the well-defined time-frequency profile in this region.

### C. Displacement gate and velocity gate

A connection between the observables and times needs to be established so that one can probe the time information through measurable quantities. Since the probe field is weak,

the ionization time  $t_i$  and the recombination time  $t_r$  are dictated by the fundamental field. To this end, the probe field should satisfy  $\epsilon \lesssim 0.1$  and we use  $\epsilon = 0.02$ . The effect of the probe field on the harmonic intensity and the amplitude ratio can be understood by a quantitative analysis [30,31] as explained in the following.

Assuming a Coulomb-free Newtonian trajectory with transverse coordinate  $y(t)$ , it is required that the transverse displacement of the electron between ionization and recollision is zero in the HHG process, namely,  $y(t_r) - y(t_i) = 0$ , so that the laser-driven electron recollides with the parent ion. To satisfy this condition, the initial transverse velocity must be

$$v_{y0} = -\frac{\epsilon E_0}{n\omega} \left( \sin(\varphi_i) + \frac{\cos(\varphi_r) - \cos(\varphi_i)}{n\omega(t_r - t_i)} \right), \quad (5)$$

with  $\varphi_i = n\omega t_i + \phi$  and  $\varphi_r = n\omega t_r + \phi$ . As confirmed in previous work [7,45], vanishing  $v_{y0}$  corresponds to the maximum of the harmonic intensity. Therefore, at the optimal phase  $\bar{\phi}_1$  maximizing the harmonic intensity, Eq. (5) implies a condition on the times  $t_i$  and  $t_r$  (displacement gate).

For linearly polarized harmonics, the  $y$ -to- $x$  amplitude ratio  $R$  is directly related to the polarization angle  $\theta$  with respect to the  $x$  direction, i.e.,  $R = \tan\theta$ . In the experiment [30],  $R$  was measured as the amplitude ratio between adjacent even and odd harmonics. This is possible because for an  $\omega$ - $2\omega$  OTC field, the time-dependent harmonic field in the  $y$  direction is  $T/2$  periodic, while the time-dependent harmonic field along the  $x$  axis undergoes a sign change from one half cycle to the next half cycle of the fundamental field. Thus, under Fourier transformation to the frequency domain, the even harmonics are polarized along  $y$  and the odd harmonics are polarized along  $x$  [30,46]. When the initial bound state possesses spherical symmetry, the harmonic polarization angle coincides with the electron return angle [46] and  $R$  can be expressed as  $|v_y(t_r)/v_x(t_r)|$ . With  $v_y(t_r)$  calculated from the Coulomb-free Newtonian motion and using  $v_x(t_r) = \sqrt{2(\Omega - I_p)}$ , this leads to

$$R = \frac{\epsilon E_0/(n\omega)}{\sqrt{2(\Omega - I_p)}} \left| \sin(\varphi_r) + \frac{\cos(\varphi_r) - \cos(\varphi_i)}{n\omega(t_r - t_i)} \right|. \quad (6)$$

Hence, when the two-color delay is adjusted such that the amplitude ratio  $R$  is maximized, Eq. (6) implies a condition on the times  $t_i$  and  $t_r$  (velocity gate).

The experiment or the TDSE solutions provide us with the optimal phase  $\bar{\phi}_1$  maximizing the harmonic intensity and the optimal phase  $\bar{\phi}_2$  maximizing the amplitude ratio for every harmonic order. From the optimal phases, we can deduce both  $t_i$  and  $t_r$  for each harmonic order using the displacement gate and the velocity gate. In our implementation [31], we allow complex times in Eqs. (5) and (6) in accordance with the quantum-orbit model, so the two retrieval equations read

$$\text{Re}v_{y0} = 0, \quad (7)$$

$$\frac{\partial R}{\partial \phi} = 0. \quad (8)$$

We have checked numerically that the optimal phases resulting from Eqs. (7) and (8) when the complex QO times are inserted are consistent with the optimal phases obtained

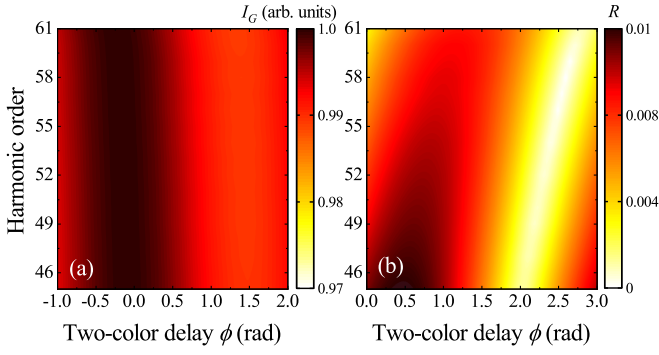


FIG. 2. (a) Normalized harmonic signal and (b) harmonic y-to-x amplitude ratio as a function of harmonic order and two-color delay. These quantities are calculated from TDSE solutions for the  $\omega$ - $2\omega$  scheme.

when the SFA model is used to calculate the two observables directly.

### III. RESULTS AND DISCUSSION

#### A. Retrieval of ionization and recombination times

We present the two observables for the long trajectory as functions of harmonic order and two-color delay in Fig. 2. Here we use an  $\omega$ - $2\omega$  field with a fundamental wavelength of 800 nm and intensity  $4.0 \times 10^{14}$  W/cm<sup>2</sup>. The harmonic intensity [Fig. 2(a)] and the y-to-x amplitude ratio [Fig. 2(b)] vary with the two-color delay. At every harmonic order, we can find the optimal phases  $\bar{\phi}_1$  and  $\bar{\phi}_2$  maximizing either of the two observables. Here  $\bar{\phi}_1$  decreases slightly with the harmonic order, while  $\bar{\phi}_2$  increases. These trends are opposite to the short-trajectory case (cf. Fig. 1 in Ref. [31]).

Our aim is to retrieve the ionization and recombination times  $t_i$  and  $t_r$  by inserting the measurable optimal phases into Eqs. (7) and (8). However, since we work with complex times, there are four unknown variables and only two equations. To overcome this problem, two approximations are adopted [31]: The imaginary part of  $t_r$  is neglected and the imaginary part of  $t_i$  is approximated as the Keldysh time at  $t_i^0 = \text{Re}t_i$ , i.e.,  $\text{Im}t_i = \sqrt{2I_p}/|E_x(t_i^0)|$  [47]. Figure 3 shows the retrieved ionization and return times from the TDSE. For comparison, the results calculated from the QO model are also presented. In the QO model, the complex times  $t_i = t_i^0 + i \text{Im}t_i$  and  $t_r = t_r^0 + i \text{Im}t_r$  are the solutions of the saddle-point equations [2]

$$\frac{\mathbf{v}^2(t_i)}{2} = -I_p, \quad \frac{\mathbf{v}^2(t_r)}{2} = \Omega - I_p, \quad (9)$$

with the velocity  $\mathbf{v}(t) = \mathbf{p}(t_i, t_r) + \mathbf{A}(t)$  and the saddle-point momentum  $\mathbf{p}(t_i, t_r) = -1/(t_r - t_i) \int_{t_i}^{t_r} \mathbf{A}(t) dt$ . Because the streaking field is weak, we neglect the y component of  $\mathbf{A}$  in the saddle-point equations unless otherwise stated. The saddle-point equations result from finding the complex stationary points of  $\Omega t_r - S_v$ , where

$$S_v(t_i, t_r) = \int_{t_i}^{t_r} dt \left( \frac{\mathbf{v}^2(t)}{2} + I_p \right). \quad (10)$$

Figure 3 shows clearly that the TDSE results for the long trajectory are in good agreement with the QO model. This means

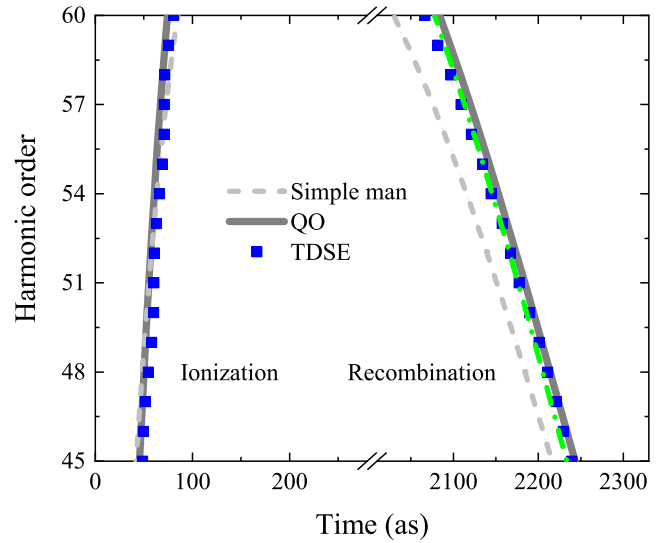


FIG. 3. Ionization and recombination times for the long trajectory in HHG: times retrieved from the  $\omega$ - $2\omega$  scheme with observables calculated from the TDSE (blue squares), times from the QO model (thick gray lines), and times from the simple man's model, i.e., the QO model with  $I_p = 0$  (light gray dashed lines). The green dash-dotted line represents the Coulomb-corrected return time estimated by the analytical  $R$ -matrix theory (see the text for details).

that we do not observe any Coulomb effects on ionization and recombination times when using the retrieval method with the  $\omega$ - $2\omega$  field.

A purely classical model with real times, known as the simple man's model, can be obtained from the QO model by setting  $I_p = 0$ . For the long trajectory considered here, the return times from the simple man's model differ significantly from the QO return times, while the ionization times are very close to those from the QO model (see Fig. 3).

#### B. Effect of Coulomb interaction on ionization time

Before analyzing the results of the time-retrieval method further, we discuss three theoretical models for the influence of the Coulomb interaction on the ionization times of the long trajectory. Only the linearly polarized fundamental field enters these models, so the electron trajectories are one dimensional. Nevertheless, we retain the vector notation in some of the equations so that they can be reused in the two-color calculations later in this section.

##### 1. Adiabatic correction

In an adiabatic picture, the tunneling through the barrier launches an electron with zero velocity, but immediately after tunneling, the electron is affected by the attractive Coulomb force. We treat the Coulomb force as a small perturbation on top of the classical electron motion induced by the laser field and furthermore we assume that the laser field is static during the short time when the Coulomb force acts. A classical evaluation gives a simple expression for the resulting

Coulomb-induced velocity change [48,49]

$$v_0^c = \frac{\pi E_0 \cos(\omega t_i^0)}{(2I_p)^{3/2}}, \quad (11)$$

which we will use as an effective initial velocity. Assuming that an electron starts with an initial velocity  $v_0^c$  along the laser field at the real time  $t_i^0$  and neglecting any further Coulomb attraction, the classical return velocity is  $v_r^e = v_0^c - \int_{t_i^0}^{t_r^0} E_x(t) dt$ . If we have a return velocity  $v_r^e$  corresponding to a set of times  $t_i^0$  and  $t_r^0$  in the Coulomb-free case ( $v_0^e = 0$ ) and if we keep both  $v_r^e$  and  $t_r^0$  fixed when the Coulomb force is taken into account ( $v_0^e = v_0^c$ ), then to first order in the Coulomb interaction, the ionization time must change by an amount  $\delta t_i^0$  that satisfies  $0 = v_0^c + E_x(t_i^0) \delta t_i^0$ . This leads to the Coulomb-induced ionization-time shift

$$\delta t_i^0 = \frac{-\pi}{(2I_p)^{3/2}}. \quad (12)$$

Hence, we estimate the ionization time as  $t_i^0 + \delta t_i^0$ , where the unperturbed time  $t_i^0$  is taken from the QO model. It is noteworthy that the estimate for the shift in Eq. (12) does not depend on the laser parameters or the harmonic order at all.

### 2. Classical model

In this model, the electron trajectory  $\mathbf{r}(t)$  follows Newton's equation

$$\ddot{\mathbf{r}}(t) = -\mathbf{E}(t) - \partial_{\mathbf{r}} V(\mathbf{r}(t)). \quad (13)$$

Here the force  $-\partial_{\mathbf{r}} V(\mathbf{r})$ , derived from the same potential as used in the TDSE, is taken into account in a nonperturbative manner after the tunneling of the electron. The initial velocity

$$\dot{\mathbf{r}}(t_i^0) = \text{Re}[\mathbf{p}(t_i, t_r) + \mathbf{A}(t_i^0)] \quad (14)$$

and the initial position

$$\mathbf{r}(t_i^0) = \text{Re} \left( \int_{t_i}^{t_i^0} [\mathbf{p}(t_i, t_r) + \mathbf{A}(t)] dt \right) \quad (15)$$

are chosen in the spirit of the QO model, i.e., the potential is neglected during tunneling. The recombination time  $t_r'$  is defined by  $\mathbf{r}(t_r') = 0$ . The return energy  $E_r$  of the electron then determines the energy  $\Omega'$  of the emitted radiation,

$$\Omega'(t_i^0, t_r') = I_p + E_r, \quad (16)$$

where the total energy

$$E_r = \frac{\dot{\mathbf{r}}^2(t_r')}{2} + V(\mathbf{r}(t_r')) \quad (17)$$

is the sum of the kinetic and potential energies. The denotations  $t_r'$  and  $\Omega'$  are used to distinguish these quantities from those of the QO model that are used in the computation of the initial conditions. The desired ionization time for each harmonic order is then given by the mapping between  $\Omega'$  and  $t_i^0$ . In the potential-free case, we have verified that for a given harmonic frequency, the real ionization and return times of the classical model (CM) agree well with the real parts from the QO model.

### 3. Analytical R-matrix method

Here we follow the theory by Torlina and Smirnova [36,50], which corrects the QO model to first order in the electron-core interaction. The relevant equations are repeated here for completeness. Note that a similar approach was discussed in [51]. In the ARM theory, the electron-core interaction is approximated as a pure Coulomb potential  $U(\mathbf{r}) = -1/\sqrt{\mathbf{r}^2}$  and a Coulomb term

$$S_c = \int_{t_k}^{t_{\text{end}}} dt U(\mathbf{r}_a(t)) \quad (18)$$

is added to the SFA action  $S_v$  of Eq. (10). Here the potential-free trajectory

$$\mathbf{r}_a(t) = \int_{t_i}^t [\mathbf{p}(t_i, t_r) + \mathbf{A}(t')] dt' \quad (19)$$

is used in the integrand. The lower limit of the integral in Eq. (18) is determined by a boundary-matching procedure. This is necessary because the ARM theory partitions the configuration space into an inner and an outer region, separated by the surface of a sphere. The boundary matching prevents that positions close to zero are inserted into the Coulomb potential. This leads to  $t_k = t_i - i/(2I_p)$  [50]. The upper limit  $t_{\text{end}}$  is found by the condition  $r_0 = \sqrt{\mathbf{r}_a^2(t_{\text{end}})}$ , meaning that at time  $t_{\text{end}}$  the electron returns to the position [36,52]

$$r_0 = \exp \left[ 2 \left( 0.5772 - \sum_{p=1}^{\infty} [1 - v_r p \arctan(1/(v_r p))] / p \right) \right] / (2v_r), \quad (20)$$

where the return velocity  $v_r = \sqrt{2(\Omega - I_p)}$  is determined by the harmonic emission frequency  $\Omega$ . One finds the first-order shifts of the real parts of the saddle-point times (for the derivation, see Appendix A in Ref. [36])

$$\Delta t_i^0 = -\frac{\partial \text{Re} S_c}{\partial I_p} - \frac{\partial \text{Re} S_c}{\partial \Omega}, \quad \Delta t_r^0 = -\frac{\partial \text{Re} S_c}{\partial \Omega}. \quad (21)$$

In practice, the derivatives are obtained by evaluating  $S_c$  for close-lying values of  $I_p$  and  $\Omega$ .

Figure 4 shows the ionization times calculated from the above theoretical models. All three models (adiabatic correction, CM, and ARM) result in a shift of about 30 as to earlier times when compared to the QO model. This result is similar to the previous finding for the short trajectory [37]. It raises the question whether the OTC ionization-time retrieval is able to measure this Coulomb-induced time delay.

In the following, the reconstruction of ionization times via the OTC scheme uses only the harmonic intensity as an observable, i.e., only the displacement gate. We do not use the velocity gate. Instead, we fix the real part of the return time to the value given by the QO model and the imaginary part is set to zero. This is justified by our finding that the retrieved return time in Fig. 3 matches well the QO return time. In the figure, we have additionally included the return time from the ARM method described above as green dash-dotted line, which also agrees well with the QO model. Furthermore, we have confirmed the validity of our approach by comparing ionization times extracted by use of only the displacement gate, i.e., Eq. (7), to those resulting from both gates, i.e., Eqs. (7) and (8).

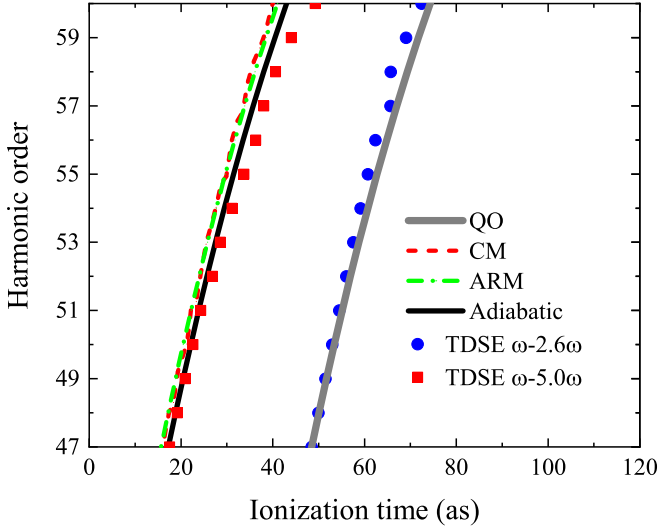


FIG. 4. Ionization times from models taking into account the Coulomb interaction: adiabatic correction (black solid line), CM (red dashed line), and ARM (green dash-dotted line). Two representative results from the TDSE-based OTC scheme are shown:  $n = 2.6$  representing streaking with low frequency and  $n = 5$  representing streaking with high frequency. The thick gray line shows the real parts of ionization times from the QO model, i.e., a model without Coulomb interaction.

Two representative results from the OTC scheme based on TDSE results using low-frequency ( $2.6\omega$ ) and high-frequency ( $5\omega$ ) streaking are presented in Fig. 4. It is found that the Coulomb-free ionization times of the QO model agree with the TDSE using the  $\omega-2.6\omega$  field, while the Coulomb-corrected ionization times are consistent with the TDSE using the  $\omega-5\omega$  field. This means that the Coulomb effect on the ionization times is hidden in the low-frequency OTC scheme, but the high-frequency OTC scheme provides a chance to retrieve the Coulomb-induced time shift. Additionally, the good agreement between classical models (adiabatic correction and CM) and the quantum-mechanical model (the ARM model) indicates that the under-barrier Coulomb influence plays a minor role. Thus, the Coulomb shift can be understood within an intuitive classical picture as follows. After tunneling, the attractive Coulomb force acts against the laser-induced acceleration of the electron. To compensate for this effect, the electron needs to start earlier so that it receives more acceleration from the driving field.

Our findings about the frequency dependence of the time retrieval are again similar to the short-trajectory case [37]. In the following, we aim to show that the origin of the frequency dependence lies in the structure of the retrieval equation and that it is not due to an inaccuracy in the TDSE solutions. To this end, we demonstrate that similar behavior is obtained when the optimal phases for the time retrieval are obtained not from the TDSE but from alternative methods. For this purpose, the CM and ARM model are generalized to OTC fields.

Similar to the one-color CM, the initial conditions in the two-color CM are taken from the QO model, but the electron trajectory  $\mathbf{r}(t)$  is now two dimensional with coordinates  $x(t)$

and  $y(t)$ . The initial positions and velocities are vectors calculated from the QO model using Eqs. (14) and (15) except that the  $y$  component of the velocity receives special treatment, as explained below. The CM does not provide a straightforward way to compute the harmonic yield, so the optimal phase  $\bar{\phi}_1$  of this model needs to be obtained in a different manner. Maximizing the harmonic intensity implies that the trajectory fulfills two conditions for the transverse motion (along the  $y$  axis): (i) The transverse coordinate of the electron returns to zero at  $t'_r$ , i.e.,  $y(t'_r) = 0$ , and (ii)  $\text{Re}v_{y0} = 0$  as in Eq. (7). The latter condition is required at the complex ionization time of the QO model and thus it brings about a condition on the initial transverse velocity  $\dot{y}(t_i^0)$  in the CM at the real time  $t_i^0$ . Using  $v_{y0} = p_y(t_i, t_r) + A_y(t_i)$  and  $\dot{y}(t_i^0) = \text{Re}[p_y(t_i, t_r) + A_y(t_i^0)]$ , we find

$$\dot{y}(t_i^0) = \text{Re}[A_y(t_i^0) - A_y(t_i)]. \quad (22)$$

In the numerical implementation of the model, we always start with the initial condition of Eq. (22) and we vary the two-color delay  $\phi$  in order to meet the return condition  $\mathbf{r}(t'_r) = 0$ . Because of the two-dimensional trajectory, the return time does not have to be exactly the same as in the one-color CM, but they are very close because the streaking field is weak.

In the two-color ARM theory, the harmonic intensity is calculated from the total ARM action which includes the Coulomb term  $S_c$  [see Eq. (18)]. Thus, the harmonic intensity is proportional to

$$I_a = |\exp[i\Omega t_r'' - iS_v(t_i'', t_r'') - iS_c(t_i'', t_r'')]|^2. \quad (23)$$

The SFA action  $S_v$  is given in Eq. (10). The expressions for the actions used in Eq. (23) are evaluated with the full two-dimensional OTC vector potential. Also, we use the OTC saddle-point times  $t_i''$  and  $t_r''$ , i.e., the solutions of Eq. (9) with both  $x$  and  $y$  components taken into account. The one-color saddle-point times  $t_i$  and  $t_r$  do not provide sufficient accuracy even though the probe field along  $y$  is small. The reason is that the Coulomb term  $\exp[-iS_c(t_i'', t_r'')]$  is very sensitive to the times because the Coulomb phase is not stationary at any of the SFA saddle points [53]. The optimal phase  $\bar{\phi}_1$  is then obtained by finding the maximum of the harmonic intensity given by Eq. (23).

Figure 5 shows the retrieved ionization time as a function of the streaking frequency for the harmonic order  $q = 53$ . All three OTC calculations (CM, ARM, and TDSE) show a double-plateau structure. In the first plateau, the retrieved ionization times agree with the QO model, i.e., the Coulomb interaction does not show in these results. In previous work on photoelectrons, a similar conclusion was drawn when orthogonal streaking was used to determine the ionization time in the case of an attoclock setup [35]. When the streaking frequency is chosen to be identical to the fundamental frequency, i.e.,  $n = 1$ , it is easy to understand that all three OTC models should predict the same optimal phase  $\bar{\phi}_1 = 0$  modulo  $\pi$  because this choice makes the total field linearly polarized, preventing any loss of harmonic yield due to lateral displacement. Indeed, the results of the numerical optimization procedure at  $n = 1$  are very close to each other and the obtained ionization times are extremely close to the time from the QO model. In contrast, the second plateau

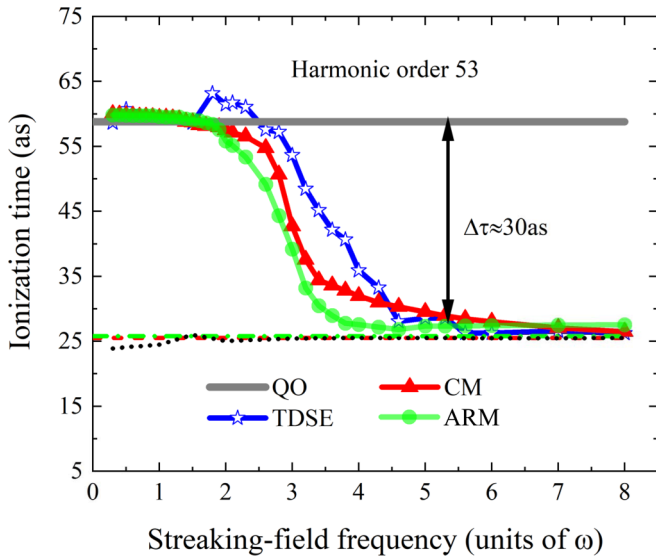


FIG. 5. Reconstructed ionization times changing with the streaking frequency  $n\omega$  for the harmonic order  $q = 53$ : TDSE (stars connected with blue lines), CM (triangles connected with red lines), and ARM (circles connected with green lines). Reference times from one-color models are shown as horizontal lines: QO (thick gray solid lines), CM (red dashed lines), and ARM (green dash-dotted lines). The black dotted line shows results from the two-color CM without the  $y$  component of the Coulomb force.

exhibits a Coulomb-induced time shift. Here the retrieved ionization times agree with the estimates from the one-color models that include the Coulomb interaction (see the horizontal lines in Fig. 5). The three OTC calculations (TDSE, CM, and ARM) differ slightly in the extension of the plateaus, but to a good approximation we can conclude that the low-frequency plateau reaches at least  $n = 2$  and the high-frequency plateau begins before  $n = 5$ . Interestingly, these values appear to be slightly higher than those found for the short trajectory in [37], where  $n = 4$  was found to be more than sufficient to resolve the Coulomb shift.

To investigate the physical origin of the difference between low-frequency and high-frequency regions, we also consider a modification of the two-color CM, where we neglect the Coulomb force along the  $y$  axis (see the black dotted curve in Fig. 5). In this case, we find an almost frequency-independent result for the retrieved ionization time at a value that is consistent with the second plateau of the TDSE calculation. This means that the OTC scheme would work accurately at any probe frequency if there was no Coulomb force along the

probe direction. Hence, the inability of the OTC method to resolve the correct time at low frequencies is caused by the Coulomb field along the probe direction, which is not taken into account in the retrieval equations.

#### IV. CONCLUSION

We have reported that the OTC probe scheme, which employs a probe field (streaking field) polarized along the direction perpendicular to the fundamental driving field, is able to measure the ionization and return times of the long trajectory in HHG. Furthermore, the classical electron-trajectory model and the quantum-mechanical theory demonstrate that the long-range electron-core interaction causes an ionization-time shift of 30 as towards earlier times for the long trajectory. In an intuitive picture, the attractive Coulomb force along the fundamental field polarization axis leads to a reduced acceleration of the outgoing electron. To compensate for this reduction, an earlier release into the field is needed. When the OTC probe scheme is applied over a wide range of streaking frequencies, the reconstructed ionization time as a function of the streaking frequency exhibits a double-plateau structure. Only in the second plateau, the Coulomb-induced time shift is revealed by the OTC scheme, whereas this time shift is absent in the first plateau. Probe frequencies of  $5\omega$  and beyond are found to be sufficient to resolve the Coulomb shift accurately. To observe the times for the long trajectory experimentally, it needs to be selected by appropriate phase-matching conditions. Notwithstanding, the outcome of the previous experiment for the short trajectory [30] indicates that under suitable conditions the times are hardly affected by macroscopic effects. Possibly, the OTC method can probe ionization and recombination times for trajectories with even longer excursion times (multiple returns), but these usually play an insignificant role in HHG under macroscopic phase-matching conditions [54,55]. Overall, streaking at various frequencies is a highly promising tool for experimental time measurements with attosecond precision.

#### ACKNOWLEDGMENTS

We thank X. Zhu for valuable discussions. This work was supported by the National Natural Science Foundation of China (Grants No. 11874030, No. 11904146, and No. 12064023), the Natural Science Foundation of Gansu Province (Grant No. 20JR5RA209), and the Scientific Research Program of the Higher Education Institutions of Gansu Province of China (Grant No. 2020A-125).

- [1] P. B. Corkum, Plasma Perspective on Strong Field Multiphoton Ionization, *Phys. Rev. Lett.* **71**, 1994 (1993).
- [2] B. C. P. Salières, L. L. Déroff, F. Grasbon, G. G. Paulus, H. Walther, R. Kopold, W. Becker, D. B. Milošević, A. Sanpera, and M. Lewenstein, Feynman's path-integral approach for intense-laser-atom interactions, *Science* **292**, 902 (2001).

- [3] K. C. Kulander, K. J. Schafer, and J. L. Krause, Dynamics of short-pulse excitation, ionization and harmonic conversion, in *Super-Intense Laser-Atom Physics*, edited by B. Pireaux, A. L'Huillier and K. Rzażewski, NATO Advanced Studies Institute, Series B: Physics (Springer, Boston, 1993), Vol. 316.
- [4] M. Lewenstein, P. Balcou, M. Y. Ivanov, A. L'Huillier, and P. B. Corkum, Theory of high-harmonic generation by low-frequency laser fields, *Phys. Rev. A* **49**, 2117 (1994).

- [5] Y. Mairesse, A. D. Bohan, L. J. Frasinski, H. Merdji, L. C. Dinu, P. Monchicourt, P. Breger, M. Kovačev, R. Taïeb, B. Carré, H. G. Muller, P. Agostini, and P. Salères, Attosecond synchronization of high-harmonic soft X-rays, *Science* **302**, 1540 (2003).
- [6] N. Dudovich, O. Smirnova, J. Levesque, Y. Mairesse, M. Y. Ivanov, D. Villeneuve, and P. B. Corkum, Measuring and controlling the birth of attosecond XUV pulses, *Nat. Phys.* **2**, 781 (2006).
- [7] F. Krausz and M. Ivanov, Attosecond physics, *Rev. Mod. Phys.* **81**, 163 (2009).
- [8] C. C. Chirilă, I. Dreisigacker, E. V. van der Zwan, and M. Lein, Emission times in high-order harmonic generation, *Phys. Rev. A* **81**, 033412 (2010).
- [9] O. Pedatzur, G. Orenstein, V. Serbinenko, H. Soifer, B. D. Bruner, A. J. Uzan, D. S. Brambila, A. G. Harvey, L. Torlina, F. Morales, O. Smirnova, and N. Dudovich, Attosecond tunnelling interferometry, *Nat. Phys.* **11**, 815 (2015).
- [10] S. Yue, S. Brennecke, H. Du, and M. Lein, Probing dynamical symmetries by bicircular high-order harmonic spectroscopy beyond the Born-Oppenheimer approximation, *Phys. Rev. A* **101**, 053438 (2020).
- [11] P. Balcou, P. Salières, A. L’Huillier, and M. Lewenstein, Generalized phase-matching conditions for high harmonics: The role of field-gradient forces, *Phys. Rev. A* **55**, 3204 (1997).
- [12] J. Itatani, J. Levesque, D. Zeidler, H. Niikura, H. Pépin, J. C. Kieffer, P. B. Corkum, and D. M. Villeneuve, Tomographic imaging of molecular orbitals, *Nature (London)* **432**, 867 (2004).
- [13] C. Vozzi, M. Negro, F. Calegari, G. Sansone, M. Nisoli, S. De Silvestri, and S. Stagira, Generalized molecular orbital tomography, *Nat. Phys.* **7**, 822 (2011).
- [14] P. M. Kraus, A. Rupenyan, and H. J. Wörner, High-Harmonic Spectroscopy of Oriented OCS Molecules: Emission of Even and Odd Harmonics, *Phys. Rev. Lett.* **109**, 233903 (2012).
- [15] M. Lein, Attosecond Probing of Vibrational Dynamics with High-Harmonic Generation, *Phys. Rev. Lett.* **94**, 053004 (2005).
- [16] S. Baker, J. S. Robinson, C. Haworth, H. Teng, R. Smith, C. C. Chirilă, M. Lein, J. Tisch, and J. P. Marangos, Probing proton dynamics in molecules on an attosecond time scale, *Science* **312**, 424 (2006).
- [17] J. P. Farrell, S. Petretti, J. Förster, B. K. McFarland, L. S. Spector, Y. V. Vanne, P. Decleva, P. H. Bucksbaum, A. Saenz, and M. Gühr, Strong Field Ionization to Multiple Electronic States in Water, *Phys. Rev. Lett.* **107**, 083001 (2011).
- [18] P. Lan, M. Ruhmann, L. He, C. Zhai, F. Wang, X. Zhu, Q. Zhang, Y. Zhou, M. Li, M. Lein, and P. Lu, Attosecond Probing of Nuclear Dynamics with Trajectory-Resolved High-Harmonic Spectroscopy, *Phys. Rev. Lett.* **119**, 033201 (2017).
- [19] O. Smirnova, Y. Mairesse, S. Patchkovskii, N. Dudovich, D. Villeneuve, P. Corkum, and M. Y. Ivanov, High harmonic interferometry of multi-electron dynamics in molecules, *Nature (London)* **460**, 972 (2009).
- [20] A. D. Shiner, B. E. Schmidt, C. Trallero-Herrero, H. J. Wörner, S. Patchkovskii, P. B. Corkum, J.-C. Kieffer, F. Légaré, and D. M. Villeneuve, Probing collective multi-electron dynamics in xenon with high-harmonic spectroscopy, *Nat. Phys.* **7**, 464 (2011).
- [21] D. Faccialà, S. Pabst, B. D. Bruner, A. G. Ciriolo, S. De Silvestri, M. Devetta, M. Negro, H. Soifer, S. Stagira, N. Dudovich, and C. Vozzi, Probe of Multielectron Dynamics in Xenon by Caustics in High-Order Harmonic Generation, *Phys. Rev. Lett.* **117**, 093902 (2016).
- [22] M. Kitzler and M. Lezius, Spatial Control of Recollision Wave Packets with Attosecond Precision, *Phys. Rev. Lett.* **95**, 253001 (2005).
- [23] M. Kitzler, X. Xie, A. Scrinzi, and A. Baltuska, Optical attosecond mapping by polarization selective detection, *Phys. Rev. A* **76**, 011801(R) (2007).
- [24] H. Niikura, H. J. Wörner, D. M. Villeneuve, and P. B. Corkum, Probing the Spatial Structure of a Molecular Attosecond Electron Wave Packet Using Shaped Recollision Trajectories, *Phys. Rev. Lett.* **107**, 093004 (2011).
- [25] D. J. Hoffmann, C. Hutchison, A. Zaïr, and J. P. Marangos, Control of temporal mapping and harmonic intensity modulation using two-color orthogonally polarized fields, *Phys. Rev. A* **89**, 023423 (2014).
- [26] X. Xie, Two-Dimensional Attosecond Electron Wave-Packet Interferometry, *Phys. Rev. Lett.* **114**, 173003 (2015).
- [27] M. Richter, M. Kunitski, M. Schöffler, T. Jahnke, L. P. H. Schmidt, M. Li, Y. Q. Liu, and R. Dörner, Streaking Temporal Double-Slit Interference by an Orthogonal Two-Color Laser Field, *Phys. Rev. Lett.* **114**, 143001 (2015).
- [28] C. Y. Zhai, X. F. Zhang, X. S. Zhu, L. X. He, Y. F. Zhang, B. N. Wang, Q. B. Zhang, P. F. Lan, and P. X. Lu, Single-shot molecular orbital tomography with orthogonal two-color fields, *Opt. Express* **26**, 2775 (2018).
- [29] D. B. Milošević and W. Becker, X-ray harmonic generation by orthogonally polarized two-color fields: Spectral shape and polarization, *Phys. Rev. A* **100**, 031401(R) (2019).
- [30] D. Shafir, H. Soifer, B. D. Bruner, M. Dagan, Y. Mairesse, S. Patchkovskii, M. Y. Ivanov, O. Smirnova, and N. Dudovich, Resolving the time when an electron exits a tunnelling barrier, *Nature (London)* **485**, 343 (2012).
- [31] J. Zhao and M. Lein, Determination of Ionization and Tunneling Times in High-Order Harmonic Generation, *Phys. Rev. Lett.* **111**, 043901 (2013).
- [32] J. Henkel and M. Lein, Analysis of electron trajectories with two-color strong-field ionization, *Phys. Rev. A* **92**, 013422 (2015).
- [33] N. Eicke and M. Lein, Extracting trajectory information from two-color strong-field ionization, *J. Mod. Opt.* **64**, 981 (2017).
- [34] X. Gong, C. Lin, F. He, Q. Song, K. Lin, Q. Ji, W. Zhang, J. Ma, P. Lu, Y. Liu, H. Zeng, W. Yang, and J. Wu, Energy-Resolved Ultrashort Delays of Photoelectron Emission Clocked by Orthogonal Two-Color Laser Fields, *Phys. Rev. Lett.* **118**, 143203 (2017).
- [35] N. Eicke, S. Brennecke, and M. Lein, Attosecond-Scale Streaking Methods for Strong-Field Ionization by Tailored Fields, *Phys. Rev. Lett.* **124**, 043202 (2020).
- [36] L. Torlina and O. Smirnova, Coulomb time delays in high harmonic generation, *New J. Phys.* **19**, 023012 (2017).
- [37] S. Yue, S. Xue, H. Du, and M. Lein, Revealing Coulomb time shifts in high-order harmonic generation by frequency-dependent streaking, *Phys. Rev. A* **105**, L041103 (2022).
- [38] D. Shafir, B. Fabre, J. Higué, H. Soifer, M. Dagan, D. Descamps, E. Mével, S. Petit, H. J. Wörner, B. Pons, N.



- Dudovich, and Y. Mairesse, Role of the Ionic Potential in High Harmonic Generation, *Phys. Rev. Lett.* **108**, 203001 (2012).
- [39] L. Brugnera, D. J. Hoffmann, T. Siegel, F. Frank, A. Zaïr, J. W. G. Tisch, and J. P. Marangos, Trajectory Selection in High Harmonic Generation by Controlling the Phase between Orthogonal Two-Color Fields, *Phys. Rev. Lett.* **107**, 153902 (2011).
- [40] C. Hofmann, A. S. Landsman, and U. Keller, Disentangling long trajectory contributions in two-colour high harmonic generation, *Appl. Sci.* **8**, 341 (2018).
- [41] X. J. Xie, C. Chen, G. G. Xin, J. Liu, and Y. J. Chen, Coulomb-induced ionization time lag after electrons tunnel out of a barrier, *Opt. Express* **28**, 33228 (2020).
- [42] J. Crank and P. Nicolson, A practical method for numerical evaluation of solutions of partial differential equations of the heat-conduction type, *Math. Proc. Cambridge* **43**, 50 (1947).
- [43] M. Nurhuda and F. H. M. Faisal, Numerical solution of time-dependent Schrödinger equation for multiphoton processes: A matrix iterative method, *Phys. Rev. A* **60**, 3125 (1999).
- [44] P. Ehrenfest, Bemerkung über die angenäherte Gültigkeit der klassischen Mechanik innerhalb der Quantenmechanik, *Z. Phys.* **45**, 455 (1927).
- [45] M. Y. Ivanov, M. Spanner, and O. Smirnova, Anatomy of strong field ionization, *J. Mod. Opt.* **52**, 165 (2005).
- [46] D. Shafir, Y. Mairesse, D. M. Villeneuve, P. B. Corkum, and N. Dudovich, Atomic wavefunctions probed through strong-field light-matter interaction, *Nat. Phys.* **5**, 412 (2009).
- [47] L. V. Keldysh, Ionization in the field of a strong electromagnetic wave, *Sov. Phys. JETP* **20**, 1307 (1965).
- [48] S. P. Goreslavski, G. G. Paulus, S. V. Popruzhenko, and N. I. Shvetsov-Shilovski, Coulomb Asymmetry in Above-Threshold Ionization, *Phys. Rev. Lett.* **93**, 233002 (2004).
- [49] N. I. Shvetsov-Shilovski, S. P. Goreslavski, S. V. Popruzhenko, and W. Becker, Capture into Rydberg states and momentum distributions of ionized electrons, *Laser Phys.* **19**, 1550 (2009).
- [50] L. Torlina and O. Smirnova, Time-dependent analytical R-matrix approach for strong-field dynamics. I. One-electron systems, *Phys. Rev. A* **86**, 043408 (2012).
- [51] S. V. Popruzhenko, Coulomb phase in high harmonic generation, *J. Phys. B* **51**, 144006 (2018).
- [52] M. Ivanov and O. Smirnova, How Accurate Is the Attosecond Streak Camera? *Phys. Rev. Lett.* **107**, 213605 (2011).
- [53] O. Kneller, D. Azoury, Y. Federman, M. Krüger, A. J. Uzan, G. Orenstein, B. D. Bruner, O. Smirnova, S. Patchkovskii, M. Ivanov, and N. Dudovich, A look under the tunnelling barrier via attosecond-gated interferometry, *Nat. Photon.* **16**, 304 (2022).
- [54] C. Jin, G. L. Wang, H. Wei, A.-T. Le, and C. D. Lin, Waveforms for optimal sub-keV high-order harmonics with synthesized two- or three-colour laser fields, *Nat. Commun.* **5**, 4003 (2014).
- [55] C. Jin and C. D. Lin, Spatially coherent high-order harmonics generated at optimal high gas pressure with high-intensity one- or two-color laser pulses, *Phys. Rev. A* **94**, 043804 (2016).